Int. J. Heat Mass Transfer. Vol. 25, No. 9, pp. 1353–1361, 1982
Printed in Great Britain

0017–9310/82/091353–09 $03.00/0
Pergamon Press Ltd.

AN ANALYTICAL INVESTIGATION ON CHF OF FLOW BOILING IN UNIFORMLY HEATED VERTICAL TUBES WITH SPECIAL REFERENCE TO GOVERNING DIMENSIONLESS GROUPS

Y. KATTO
Department of Mechanical Engineering, University of Tokyo, Hongo, Bunkyo-ku, Tokyo, Japan

(*Received* 17 *March* 1982)

Abstract—Among the four characteristic regimes, which have been classified in the author's preceding study on the generalized correlation of critical heat flux (CHF), two regimes called L and H regime are ascertained to have an annular flow pattern at the tube exit. Then, employing the annular flow model developed by Whalley *et al.*, theoretical analyses are made for uniformly heated tubes fed with saturated water, R-12 and liquid nitrogen, and the results obtained are compared with the author's generalized correlation clarifying the roles of the governing dimensionless groups. It is found that the dimensionless groups adopted in Ahmad's modeling law accord with the annular flow model of Whalley *et al.*, that a special dimensionless group $\sigma\rho_l/G^2l$ can be used with a physical meaning in correlating CHF data, and that the droplet mass transfer between the liquid film and the gas core assumes different aspects between L and H regimes.

NOMENCLATURE

c_{pl}, specific heat of liquid at constant pressure [J kg^{-1} K^{-1}];
C, dimensionless constant in equation (5), or concentration of droplets in gas core [kg m^{-3}];
C_{eq}, C for hydrodynamic equilibrium [kg m^{-3}];
d, tube diameter [m];
D, deposition rate of droplets [kg m^{-2} s^{-1}];
E, entrainment rate of droplets [kg m^{-2} s^{-1}];
f, friction factor;
g, acceleration due to gravity [m s^{-2}];
G, mass velocity $W/(\pi d^2/4)$ [kg m^{-2} s^{-1}];
G_{lF}, liquid film mass velocity $W_{lF}/(\pi d^2/4)$ [kg m^{-2} s^{-1}];
H_{fg}, latent heat of evaporation [J kg^{-1}];
ΔH_i, inlet subcooling enthalpy [J kg^{-1}];
k_d, deposition mass transfer coefficient [m s^{-1}];
k_l, thermal conductivity of liquid [W m^{-1} K^{-1}];
l, heated tube length [m];
m, liquid film thickness [m];
p, absolute pressure [bar];
q, heat flux [W m^{-2}];
q_c, critical heat flux [W m^{-2}];
q_{co}, q_c at $\Delta H_i = 0$;
Re, Reynolds number;
W, total mass flow rate [kg s^{-1}];
W_{lF}, mass flow rate of liquid film [kg s^{-1}];
z, distance along tube [m].

Greek symbols

α, void fraction of gas core;
μ_l, viscosity of liquid [Pa s];
μ_v, viscosity of vapor [Pa s];
ρ_l, density of liquid [kg m^{-3}];
ρ_v, density of vapor [kg m^{-3}];
σ, surface tension [N m^{-1}];
τ_i, interfacial shear stress [N m^{-2}];
Φ, relative net deposition rate defined in equation (15);
χ, quality;
χ_{ex}, exit quality at CHF condition.

1. INTRODUCTION

CRITICAL heat flux (CHF) of forced convective boiling is a phenomenon related to the design and safety of various important devices such as nuclear reactors, steam generators, superconducting magnets and liquid fuel rocket engines. There is also a necessity to study a given system by using an expedient fluid rather than the working fluid. Therefore, in spite of the involved situation and the accompanying difficulty, some studies have so far been made on the fluid modeling technique and generalized CHF correlation.

As for fluid modeling, it is well known that there are two types of approach: the empirical parameter approach initiated by Stevens and Kirby [1] and the dimensional analysis approach initiated by Barnett [2]. Among many proposed modeling laws, however, one of the most excellent is that of Ahmad [3], where the following dimensionless relationship for critical heat flux q_c is assumed under fixed conditions of ρ_v/ρ_l, l/d and $\Delta H_i/H_{fg}$:

$$\left.\begin{aligned} &\frac{q_c}{GH_{fg}} = f(\xi_{CHF}) \\ &\text{where } \xi_{CHF} \text{ is the modeling parameter defined as} \\ &\xi_{CHF} = \left(\frac{\sigma\rho_l}{G^2 d}\right)\left(\frac{Gd}{\mu_l}\right)^{0.5}\left(\frac{\mu_l}{\mu_v}\right)^{0.3}. \end{aligned}\right\} \quad (1)$$

Equation (1) has been shown by Ahmad to apply for

water, R-12, R-22, R-113, carbon dioxide and potassium in the ranges of $\rho_v/\rho_l < 0.143$, $l/d = 59$–309 and $\Delta H_i/H_{fg} < 0.446$.

On the subject of a generalized CHF correlation, there are some pioneer studies [4, 5, 6], but succeeding studies do not seem so numerous. Recently, however, Katto [7, 8] and Shah [9] presented, almost simultaneously, generalized correlations of CHF of flow boiling in uniformly heated vertical tubes. In the Katto correlation [10], the following rather simple relationship is assumed:

$$\frac{q_c}{GH_{fg}} = f\left(\frac{\rho_v}{\rho_l}, \frac{l}{d}, \frac{\Delta H_i}{H_{fg}}, \frac{\sigma\rho_l}{G^2 l}\right) \tag{2}$$

where $\sigma\rho_l/G^2 l$ is a special dimensionless group, that is defined with the tube length l instead of the tube diameter d and has not yet been employed elsewhere in the analysis of two-phase flow (cf. [11, 12]). Meanwhile, the Shah correlation is constructed with the dimensionless groups q_c/GH_{fg}, p_r (reduced pressure in place of ρ_v/ρ_l), l/d and $\Delta H_i/H_{fg}$ together with the following dimensionless parameter:

$$Y = \left(\frac{Gc_{pl}d}{k_l}\right)\left(\frac{G^2}{\rho_l^2 gd}\right)^{0.4}\left(\frac{\mu_l}{\mu_v}\right)^{0.6} \tag{3}$$

Though comparatively recent studies are involved, there remain wide differences between equations (1)–(3). Therefore, it is necessary to discover whether there is any underlying or internal relation between them. Fortunately, Whalley *et al.* [13, 14] have recently made a comprehensive study of the theoretical model to predict CHF under annular flow conditions. There are also more recent models [15, 16] which depend on a detailed analysis of the droplet concentration in the gas core for hydrodynamic equilibrium. Other, different, models also exist [17, 18]. However, the preceding model of Whalley *et al.*, is simple and yet can predict CHF reasonably well in a wide range of conditions. In this paper, therefore, the model of Whalley *et al.* is employed to study the roles of the governing dimensionless groups. For simplification purposes, the discussion is restricted to CHF in uniformly heated tubes with saturated inlet.

2. IDENTIFICATION OF ANNULAR FLOW REGION

Comparison between experimental CHF data and annular flow model predictions is meaningless unless the data have been confirmed to belong to the annular flow region. Therefore, a preliminary study is made in this section.

2.1. *The author's generalized correlation of CHF data*

Figure 1 is a reproduction of part of the results obtained in the author's preceding report [19], where the existing data of q_{co} (critical heat flux for $\Delta H_i = 0$) obtained for various kinds of fluids are correlated. As is seen in Fig. 1, the author's generalized correlation classifies CHF data into four characteristic regimes called L, H, N and HP. L, H and N regimes correspond to the states of low, middle and high mass velocities respectively (Fig. 1). The N regime is distinguished by showing a non-linear relationship between q_c and ΔH_i. The HP regime is a special regime and occurs instead of the N regime at extremely high pressures. The correlation curves (a)–(f) in Fig. 1 are formulated as follows:

L regime.

$$\text{(a)}\quad \frac{q_{co}}{GH_{fg}} = 0.25\left(\frac{1}{l/d}\right), \tag{4}$$

$$\text{(b)}\quad \frac{q_{co}}{GH_{fg}} = C\left(\frac{\sigma\rho_l}{G^2 l}\right)^{0.043}\left(\frac{1}{l/d}\right), \tag{5}$$

where $C = 0.25$ for $l/d < 50$, $C = 0.34$ for $l/d > 150$, and $C = 0.25 + 0.0009[(l/d) - 50]$ for $l/d = 50$–150.

H and N regimes.

$$\text{(c)}\quad \frac{q_{co}}{GH_{fg}} = 0.10\left(\frac{\rho_v}{\rho_l}\right)^{0.133}\left(\frac{\sigma\rho_l}{G^2 l}\right)^{1/3}\frac{1}{1 + 0.0031(l/d)}, \tag{6}$$

$$\text{(d)}\quad \frac{q_{co}}{GH_{fg}} = 0.098\left(\frac{\rho_v}{\rho_l}\right)^{0.133}\left(\frac{\sigma\rho_l}{G^2 l}\right)^{0.433} \times \frac{(l/d)^{0.27}}{1 + 0.0031(l/d)}. \tag{7}$$

HP regime.

$$\text{(e)}\quad \frac{q_{co}}{GH_{fg}} = 0.0384\left(\frac{\rho_v}{\rho_l}\right)^{0.60}\left(\frac{\sigma\rho_l}{G^2 l}\right)^{0.173} \times \frac{1}{1 + 0.280(\sigma\rho_l/G^2 l)^{0.233}(l/d)}. \tag{8}$$

In the above, equation (7) applies to both H and N regimes [see line (d) in Fig. 1], whose boundary is given by

$$\text{(f)}\quad \frac{\sigma\rho_l}{G^2 l} = \left(\frac{0.77}{l/d}\right)^{2.70} \tag{9}$$

2.2. *Annular flow region*

Figure 2 is a reproduction of part of the results obtained in the author's preceding report [20], illus-

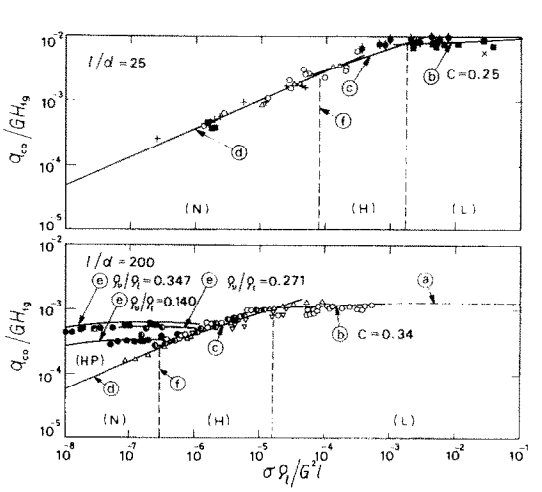

FIG. 1. Generalized correlation of q_{co} data [lines (c) and (d) represent equations (6) and (7) with $\rho_v/\rho_l = 0.048$].

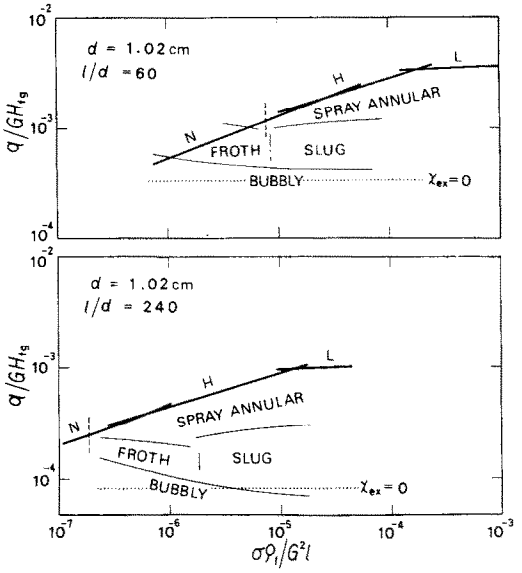

FIG. 2. Flow pattern at the exit end of uniformly heated vertical tube.

trating flow patterns measured by Bergles and Suo [21] at the exit end of uniformly heated tubes fed with water at 69 bar and $\Delta H_i/H_{fg} = 0.08$. Meanwhile, heavy lines marked with L, H and N in Fig. 2 are the boundaries due to CHF predicted by the author's generalized correlation and the vertical broken short line dividing the H and N regimes is given by equation (9). In Fig. 2, CHF in the L and H regimes is seen to take place under annular flow conditions, while CHF in the N regime is concerned with a frothy or bubbly flow pattern.

However, it is desirable to ascertain the preceding character more generally. Figure 3 is the Hewitt–Roberts map for the flow pattern of vertical two-phase flow ([22], or p. 28 of ref. [23]), on which the boundary line between the H and N regimes can be drawn in the following manner. Substituting $\sigma\rho_l/G^2l$ of equation (9) into the RHS of equation (7), and taking into account the heat balance equation for $\Delta H_i = 0$,

$$\chi = \frac{4q_{co}}{GH_{fg}}(l/d), \tag{10}$$

yields immediately the following results:

$$\frac{\chi^2G^2}{\rho_v} = 0.169\left(\frac{\sigma}{d}\right)\left(\frac{\rho_v}{\rho_l}\right)^{-0.734}\frac{(l/d)^{1.90}}{[1+0.0031(l/d)]^2} \tag{11}$$

and

$$\frac{(1-\chi)^2G^2}{\rho_l} = 2.03\left(\frac{\sigma}{d}\right)\left[1-0.288\left(\frac{\rho_v}{\rho_l}\right)^{0.133}\times\frac{(l/d)^{0.101}}{1+0.0031(l/d)}\right]^2(l/d)^{1.70}. \tag{12}$$

If fluid substance, pressure and d are specified, then equations (11) and (12) are related through (l/d) as a parameter.

Three light curves in Fig. 3 are thus obtained for water at 69 bar and $d = 5$, 12.6 and 25 mm, for which (l/d) varies from 20 to 500, that being the ordinary experimental range. Similarly, three light curves drawn in Fig. 4 are the boundaries predicted by equations (11) and (12) for water, R-12, and liquid nitrogen at $\rho_v/\rho_l = 0.048$ and $d = 8$ mm, while a dotted curve and a dot-dash curve in Fig. 4 are the boundaries for water at 29.5 and 134 bar respectively (l/d varies from 20 to 500 in all cases).

Though there are some dispersions depending on the change of pressure, diameter and substance, it may be concluded from the preceding results of Figs. 3 and 4 that L and H regimes correspond to the annular flow, while the N regime to the wispy annular flow, where agglomeration of liquid phase occurs leading to large lumps of liquid in the gas core.

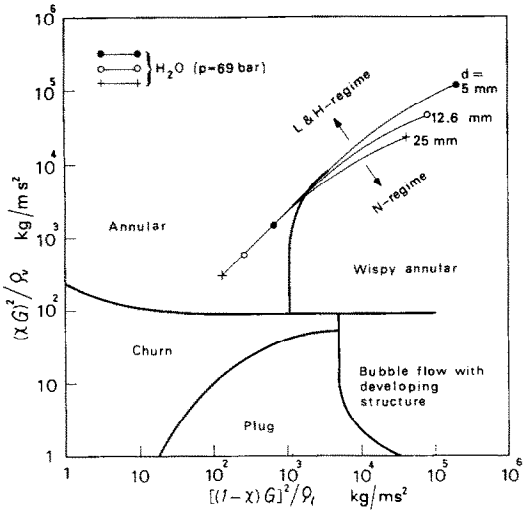

FIG. 3. Hewitt–Roberts map for flow pattern of vertical two-phase flow.

3. ANNULAR FLOW MODEL CALCULATION OF CHF

3.1. *Theoretical model of Whalley* et al.

For the change of liquid film flow rate G_{lF} along a heated tube (see Nomenclature for the definition of G_{lF}), Whalley *et al.* [13, 14] assume the following mass balance equation:

$$\frac{dG_{lF}}{dz} = \frac{4}{d}\left(D - E - \frac{q_{co}}{H_{fg}}\right) \tag{13}$$

where D and E are the local rate of droplet deposition and that of droplet entrainment per unit area of tube wall respectively, and q_{co}/H_{fg} is the evaporation rate of liquid per unit area of tube wall. Then, if the deposition mass transfer coefficient k_d is introduced, D and E are written as follows: $D = k_dC$ and $E = k_dC_{eq}$, where C is the droplet concentration in the gas core, and C_{eq} is the value of C for hydrodynamic equilibrium.

Now, in the case of a uniformly heated tube with ΔH_i

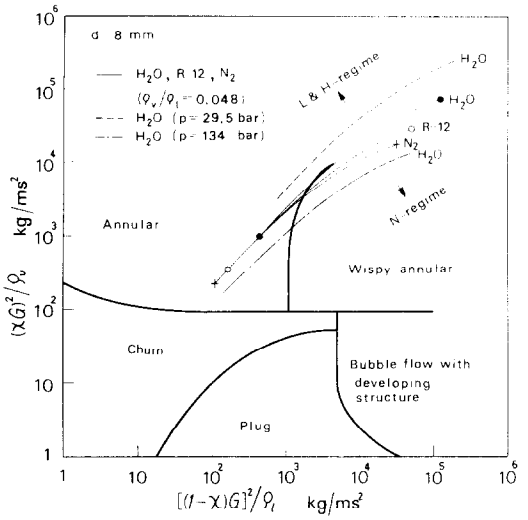

FIG. 4. Hewitt–Roberts map for flow pattern of vertical two-phase flow.

$= 0$, the local vapor quality χ at z is given via the heat balance as

$$\chi = \left(\frac{4q_{co}}{GH_{fg}}\right)\left(\frac{z}{d}\right). \tag{14}$$

Therefore, substituting χ of equation (14) for z in equation (13), and rewriting equation (13) in a dimensionless form gives immediately

$$\left.\begin{aligned} \frac{d(G_{lF}/G)}{d\chi} &= \Phi - 1 \\ \text{where} \qquad \Phi &= \frac{k_d\rho_l/G}{q_{co}/GH_{fg}}\left(\frac{C}{\rho_l} - \frac{C_{eq}}{\rho_l}\right), \end{aligned}\right\} \tag{15}$$

Φ being the net disposition rate (= deposition rate − entrainment rate) defined to take a relative value against the value of unity of the evaporation rate. The values of k_d, C and C_{eq} are given as follows.

First, empirical values of k_d given by Whalley *et al.* for water, R-12 and liquid nitrogen ([13] and p. 293 of ref. [23]) are correlated in the present paper as follows:

$$\left.\begin{aligned} k_d[\mathrm{m\,s^{-1}}] &= 0.405\,\sigma^{0.913} \\ &\qquad \text{for } \sigma < 0.0383\,[\mathrm{N\,m^{-1}}] \\ k_d[\mathrm{m\,s^{-1}}] &= 9.48 \times 10^4\,\sigma^{4.70} \\ &\qquad \text{for } \sigma > 0.0383[\mathrm{N\,m^{-1}}] \end{aligned}\right\} \tag{16}$$

where σ is the surface tension. Next, by assuming a homogeneous mixed condition of the gas core, C is given theoretically as

$$C = \rho_l(\rho_v/\rho_l)\Big/\left[\left(\frac{\chi}{1-\chi-(G_{lF}/G)}\right) + \left(\frac{\rho_v}{\rho_l}\right)\right]. \tag{17}$$

Finally, empirical values of C_{eq} given by Whalley *et al.* [14], are correlated in the present paper as follows:

$$\left.\begin{aligned} C_{eq}[\mathrm{kg\,m^{-3}}] &= 1.01 \times 10^3[(\tau_i m)/\sigma]^{2.50} \\ &\qquad \text{for } (\tau_i m)/\sigma < 0.0366 \\ C_{eq}[\mathrm{kg\,m^{-3}}] &= 1.03 \times 10^2[(\tau_i m)/\sigma]^{1.81} \\ &\qquad \text{for } 0.0366 < (\tau_i m)/\sigma < 0.247 \\ C_{eq}[\mathrm{kg\,m^{-3}}] &= 10^{(0.439+1.92(\tau_i m)/\sigma)} \\ &\qquad \text{for } 0.247 < (\tau_i m)/\sigma \end{aligned}\right\} \tag{18}$$

where τ_i is the shear stress acting on the interface between the gas core and the liquid film, and m the thickness of liquid film.

The dimensionless group $(\tau_i m)/\sigma$ used in equation (18) can be rewritten as

$$\frac{\tau_i m}{\sigma} = \left[\left(\frac{\tau_i\rho_l}{G^2}\right)\left(\frac{m}{d}\right)\right]\Big/\left(\frac{\sigma\rho_l}{G^2 d}\right) \tag{19}$$

where two dimensionless groups $(\tau_i\rho_l)/G^2$ and m/d can be evaluated, corresponding to the local values of χ and G_{lF}/G, as the roots of the following two simultaneous equations*:

$$\frac{m}{d} = \frac{G_{lF}}{G}\left(\frac{f_l/4}{\tau_i\rho_l/G^2}\right)^{1/2}, \tag{20}$$

with $f_l = 16/Re$ for $Re < 2000$, and $f_l = 0.079/Re^{1/4}$ for $Re > 2000$, where $Re = (Gd/\mu_l)(G_{lF}/G)$, and

$$(m/d) = \frac{(\rho_v/\rho_l)(\tau_i\rho_l/G^2)/180}{f_{gc}\left(1-\frac{G_{lF}}{G}\right)\left[\chi\left(1-\frac{\rho_v}{\rho_l}\right)+\frac{\rho_v}{\rho_l}\left(1-\frac{G_{lF}}{G}\right)\right]} - \frac{1}{360} \tag{21}$$

with $f_{gc} = 0.079/Re_{gc}^{1/4}$, where $Re_{gc} = (Gd/\mu_l/\mu_v)[1-(G_{lF}/G)]$.

Now, for a prescribed value of $q_{co}/(GH_{fg})$, the axial variation of G_{lF}/G can be calculated by the differential equation (15), and the CHF condition is assumed to take place at the position of $G_{lF}/G = 0$. Thus, if z/d determined from χ at $G_{lF}/G = 0$ through equation (14) agrees with l/d, then the preceding value of $q_{co}/(GH_{fg})$ is regarded as the solution. Thus, the solution of equations (14)–(21) has the following functional relationship:

$$(l/d) = f\left(\frac{q_{co}}{GH_{fg}}, \frac{\rho_v}{\rho_l}, \frac{\sigma\rho_l}{G^2 d}, \frac{Gd}{\mu_l}, \frac{\mu_l}{\mu_v}, \sigma, \rho_l, G\right) \tag{22}$$

where σ, ρ_l and G on the RHS are the quantities mainly related to the term $(k_d\rho_l)/G$ in equation (15), and

* Equation (20) is obtained from the Turner–Wallis equation $(1-\alpha) = [(dp/dz)_{lF}/(dp/dz)]^{1/2}$ with approximations of $\alpha \simeq 1 - (4m/d)$ and $dp/dz \simeq -4\tau_i/d$, while equation (21) is the Wallis equation of gas core flow.

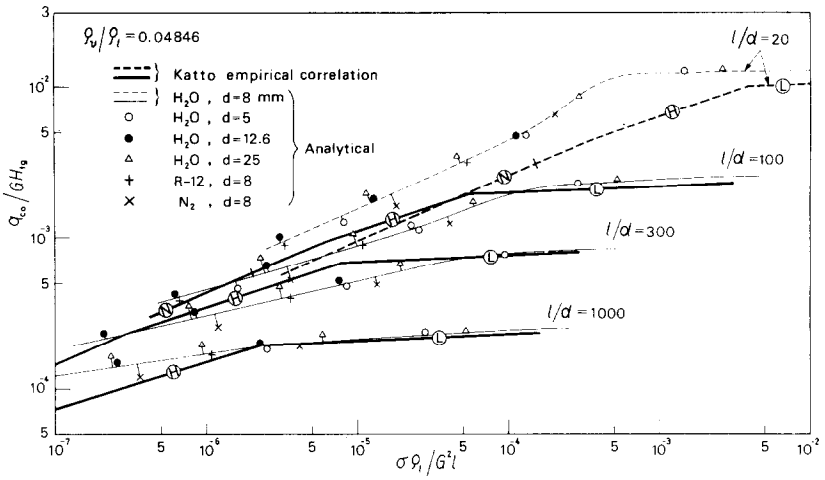

FIG. 5. Comparison between generalized correlation and numerical solution for q_{co}.

remain nongeneralized due to the empirical expression of k_d in equation (16).

3.2. *Numerical results*

In the present study, the differential equation (15) is solved on the computer by the Adams–Moulton method [24], a predictor–corrector method. For the initial state of annular flow [i.e. the starting point of the computation of equation (15)] Whalley *et al.* [13, 14] employed the conditions of $\chi = 0.01$ and $G_{lF}/G = 0.0099$. However, this value of G_{lF}/G is generally too low (see the magnitudes of G_{lF}/G near $\chi/\chi_{ex} = 0$ in Fig. 8), and sometimes causes inconvenience in the calculation process. In the present study, therefore, the value of G_{lF}/G satisfying the condition of $C = C_{eq}$ at the starting point of $\chi = 0.01$ is employed as the initial value of G_{lF}/G.

Thus, in Fig. 5, heavy (broken and solid) lines illustrate the author's generalized correlation equations (7)–(9) for $\rho_v/\rho_l = 0.04846$ and $l/d = 20, 100, 300$ and 1000, while light (broken and solid) lines represent the numerical solutions of differential equation (15) for water under the same conditions as above plus $d = 8$ mm. From the comparisons in the range of L and H regimes, it may be concluded that though a remarkable deviation is noted for $l/d = 20$, comparatively good agreements are recognized in the range of $l/d \geqslant 100$.

Next, the symbols ○, ● and △ in Fig. 5 represent the numerical solutions of differential equation (15) for water under the same conditions as before except for $d = 5$, 12.6 and 25 mm. Some discrepancies appear due to the change of tube diameter d, but they are not remarkable if the range of d is limited to an ordinary experimental range, say, 4–30 mm.

Meanwhile, the symbols + and × in Fig. 5 represent the numerical solutions of the differential equation (15) for R-12 and liquid nitrogen respectively in the case of $d = 8$ mm. As compared with the result for water under the same conditions, the solution of R-12 is located very near that of water, and the solution of liquid nitrogen is somewhat lower than that of water.

Then, the effect of ρ_v/ρ_l is also examined as shown in Fig. 6, where heavy (broken and solid) lines show the generalized correlation equations (7)–(9), while light (broken and solid) lines represent the numerical solutions of differential equation (15) for water with $d = 8$ mm. Similar conclusions to Fig. 5 may be drawn from Fig. 6 that the range of $l/d \geqslant 100$ exhibits a fairly good agreement for L and H regimes.

4. DISCUSSION ON DIMENSIONLESS GROUPS

If the nongeneralized quantities σ, ρ_l and G are ignored in equation (22), the remaining dimensionless groups are quite the same as those adopted by Ahmad [3] in constructing his modeling law. Then the three dimensionless groups $\sigma\rho_l/(G^2l)$, $(Gd)/\mu_l$ and μ_l/μ_v composing the modeling parameter ξ_{CHF} in equation (1) are the quantities governing the local value of C_{eq} of equation (18), that is, $\sigma\rho_l/(G^2d)$ exerts its effect on C_{eq} through equation (19), while $(Gd)/\mu_l$ and μ_l/μ_v exert effects through the friction factors f_l in equation (20) and f_{gc} in equation (21). In this case, however, μ_l/μ_v is included in f_{gc} as $(\mu_l/\mu_v)^{0.25}$, and accordingly the effect of μ_l/μ_v is regarded as comparatively small*. The effect of $(Gd)/\mu_l$ is also comparatively small except under the condition of very low G_{lF}/G. Finally, $(\sigma\rho_l)/(G^2d)$ can have a strong effect on C_{eq}, but in the part of the tube where the liquid film becomes so thin that $C \gg C_{eq}$ in equation (15) Φ is hardly affected by C_{eq}.

Meanwhile, as mentioned in Section 3.1, the nongeneralized quantities σ, ρ_l and G in equation (22) are mainly related to the term $(k_d\rho_l)/G$, which governs directly the magnitude of Φ. Since k_d, the deposition coefficient, is invariant, the term $(k_d\rho_l)/G$ is kept constant through the tube. This has a direct influence on the evaluation of the distance up to the position of $G_{lF}/G = 0$. Presumably, therefore, there is a possibility

* It may be of interest to note that the effect of μ_v is not included explicitly in both the theoretical models of Würtz [15] and Levy *et al.* [16].

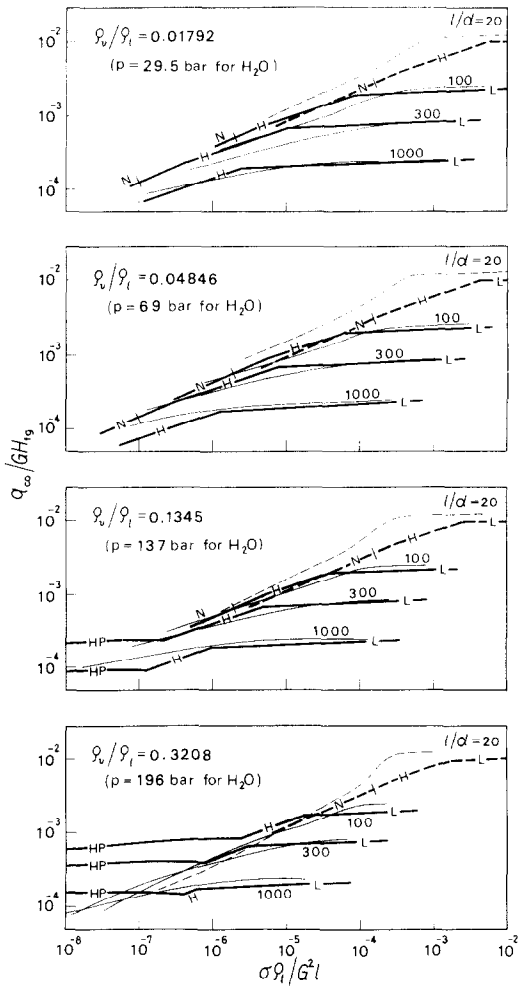

FIG. 6. Comparison between generalized correlation and numerical solution (water, d = 8 mm) for q_{co}.

that the quantities σ, ρ_l and G may cooperate with the tube length l in constructing a dimensionless group $(\sigma\rho_l)/(G^2l)$, though it be in an approximate sense.

It has been shown in Section 3.2 that when the numerical solutions of CHF are correlated in terms of $(\sigma\rho_l)/(G^2l)$ as in Fig. 5, some discrepancies arise according to the change of tube diameter and fluid substance. However, if the range of ordinary experimental conditions is considered, the discrepancies are not so remarkable, and in this sense, the availability of $(\sigma\rho_l)/(G^2l)$ in correlating CHF data can be said to be supported by the analysis based on the annular flow model of Whalley *et al.*

Finally, the dimensionless groups $(Gc_{pl}d)/k_l$ and $G^2/(\rho_l^2gd)$, composing the parameter Y of equation (3), have no connection with the theoretical model of Whalley *et al.*, though the model has not been completed theoretically, nongeneralized parts remaining. Accordingly, as far as the physical meaning of dimensionless group is concerned, the Shah correlation may stand on an unsound basis in the annular flow region at least.

5. OTHER RELATED MATTERS

5.1. *Difference in fluid behavior between L and H regimes*

Figure 7 shows the axial variations of G_{lF}/G calculated by the differential equation (15) for water at 69 bar and d = 8 mm, and Fig. 8 shows the corresponding variation of the net deposition rate of droplets Φ, which takes a relative value against the value of unity of the evaporation rate of liquid in equation (15).

In both diagrams of Fig. 7, four (two light and two heavy) curves are represented for $(\sigma\rho_l)/(G^2l)$ increased successively by about 10 times, and they are divided into two groups as follows. First, when $(\sigma\rho_l)/(G^2l)$ is comparatively high (that is L regime), G_{lF}/G takes a value of almost unity near the tube inlet, and thereafter, decreases almost linearly up to the tube exit where G_{lF}/G vanishes. This means that most of the liquid fed to the tube is wasted away by evaporation from the liquid film, and thereby the CHF condition is introduced. Therefore, this type of CHF can be said to be 'evaporation controlled'. In fact, according to Fig. 8, when $(\sigma\rho_l)/(G^2l)$ is high, either the absolute value of Φ is maintained near zero throughout the tube, or $\Phi < 0$ in the first half of the tube while $\Phi > 0$ in the second half. Either case is in accord with the circumstance that the ultimate extinction of the liquid film flow is brought about mainly through the evaporation. Table 1 shows that exit quality χ_{ex} is near unity in this high $(\sigma\rho_l)/(G^2l)$ region, corresponding to the L regime [see equations (4) and (10)].

On the other hand, when $(\sigma\rho_l)/(G^2l)$ is compara-

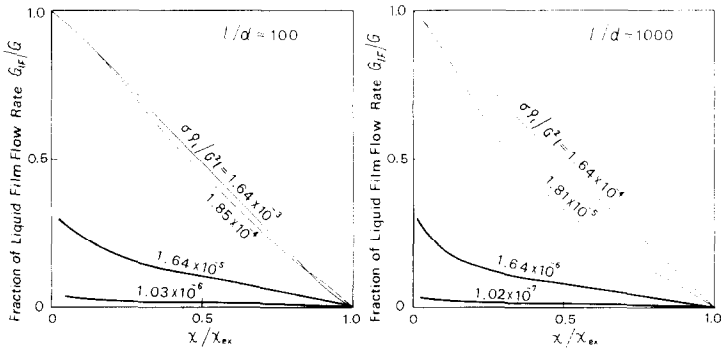

FIG. 7. Axial variation of G_{lF}/G (water, p = 69 bar, d = 8 mm).

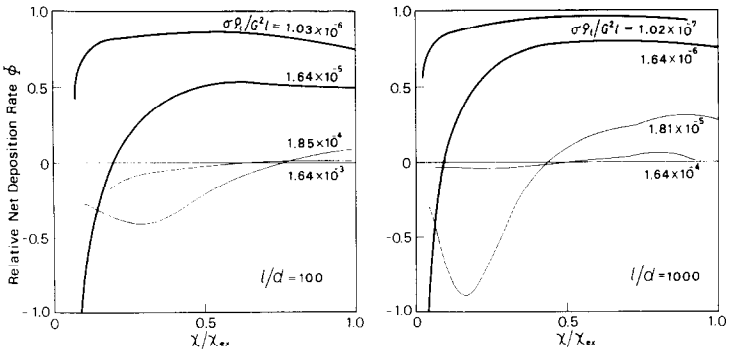

FIG. 8. Axial variation of Φ (water, $p = 69$ bar, $d = 8$ mm).

Table 1. Exit quality χ_{ex}

$l/d = 100$		$l/d = 1000$	
$\sigma\rho_l/G^2l$	χ_{ex}	$\sigma\rho_l/G^2l$	χ_{ex}
1.64×10^{-3}	1.00	1.64×10^{-4}	1.00
1.85×10^{-4}	0.88	1.81×10^{-5}	0.95
1.64×10^{-5}	0.41	1.64×10^{-6}	0.73
1.03×10^{-6}	0.18	1.02×10^{-7}	0.46

tively low (H regime), the value of G_{lF}/G is much lower than unity from near the tube inlet. In addition, Fig. 8 shows that in this low $(\sigma\rho_l)/(G^2l)$ region, Φ has the trend of being greatly negative in the vicinity of the tube inlet, and taking values near unity all through the remaining part of the tube. This means that a great part of liquid is entrained into the gas core near the tube inlet, and thereafter the liquid film is continually supplied with liquid from the gas core so as to balance nearly the local evaporation rate. Therefore, CHF in this region can be said to be 'net deposition controlled'. Table 1 shows that CHF in this region occurs with χ_{ex} much less than unity, corresponding to the H regime.

Supplementary note. There is a well-known diagram given by Hewitt (see p. 285 of ref. [23] and p. 228 of ref. [26]), which shows that the entrained droplet flow rate increases in the first part of a tube, and thereafter decreases up to the position where the entrained flow rate agrees with the liquid flow rate in the tube to generate the CHF condition. This circumstance is the same as that of the evaporation controlled CHF ($\Phi < 0$ in the first part and $\Phi > 0$ in the second part). In fact, the preceding Hewitt diagram was obtained from the experiment in the L regime.

5.2. *H regime for very high* l/d *ratios*

According to Figs. 5 and 6, in the case of the H regime for $l/d = 1000$ there is a difference in trend between the author's correlation and the numerical solution. Relating to this problem, Fig. 9 shows critical heat flux q_c against the exit quality χ_{ex} for water at $p = 69$ bar, $d = 8$ mm and $G = 2000\ \mathrm{kg\,m^{-2}\,s^{-1}}$, where a heavy line represents the author's generalized correlation equations (6) and (7) (the broken part is the N regime and the solid part the H regime), and a light line represents the numerical solution of differential equation (15)*, with six representative values of l/d along each line. Figure 9 also shows experimental data from the U.S.S.R. standard table of CHF for water at 69 bar with $d = 8$ mm [26] and from the experiment of Würtz for water at 70 bar with $d = 10$ mm [15].

The experimental data (Fig. 9) agree well with the author's correlation equations in the range of $l/d < 600$, but a separation appears for $l/d > 600$ (see [27] also). In the range of $l/d > 600$, experimental data exhibit the trend that $q_c \to 0$ and $\chi_{ex} \to 1$ with increasing l/d, for which the author's correlation becomes invalid, while the numerical solution of differential equation (15) is valid. Therefore, annular

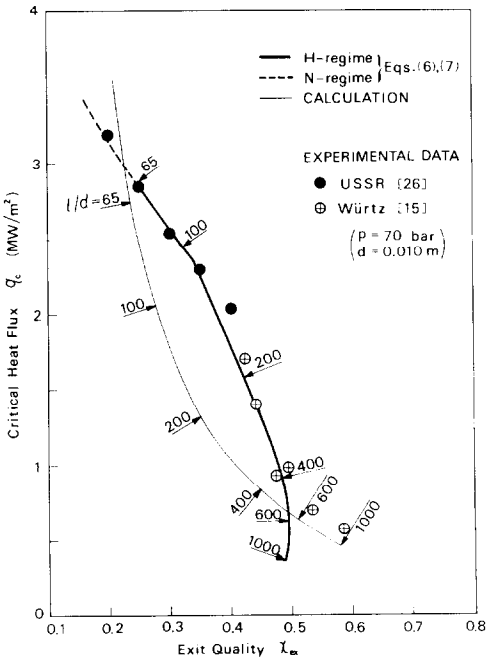

FIG. 9. Relation between q_c and χ_{ex} (water, $p = 69$ bar, $d = 8$ mm, $G = 2000\ \mathrm{kg\,m^{-2}\,s^{-1}}$).

* The boiling length concept presumably applies well to CHF in annular flow region. Accordingly, the relationship between q_c and χ_{ex} is obtainable with tolerable accuracies from the results for $\Delta H_i = 0$.

flow model calculation is regarded as useful to predict CHF in the H regime for $l/d > 600$.

5.3. *Annular flow models*

Levy *et al.* [16] has shown that their own model gives a numerical solution which has a rather similar shape to the light curve in Fig. 9 but shifts to the right so as to pass along the whole data points of Würtz. If comparison is made with the author's generalized correlation in the form of Fig. 5, good agreement is found in the L regime, but deviation appears in the H regime increasing more and more with decreasing l/d ratio. The model of Würtz [15] also exhibits rather similar characteristics to the above. Strictly speaking, therefore, there seems to remain the problem of finding the region to which annular flow models with the CHF condition of $G_{\mathrm{II}}/G = 0$ apply correctly.

6. CONCLUSIONS

Numerical analysis of CHF based on the annular flow model of Whalley *et al.* is employed together with the author's generalized correlation of CHF in the L and H regimes (annular flow region) clarifying the roles of governing dimensionless groups (Section 4). A few other related subjects, including the difference in droplet mass transfer behavior between the L and H regimes, are also investigated (Section 5).

The situation of CHF in the N and HP regimes is beyond the scope of the present study and remains to be studied in the future.

Acknowledgement—The author acknowledges the financial support given by the Ministry of Education, Science and Culture to this study [Special Project Research on Energy No. 56040014 (1981)].

REFERENCES

1. G. F. Stevens and G. J. Kirby, A quantitative comparison between data for water at 1000 psia and Freon-12 at 155 psia, uniformly heated round tubes, vertical upflow, AEEW-R 327 (1964).
2. P. G. Barnett, The scaling of forced convection boiling heat transfer, AEEW-R 134 (1963).
3. S. Y. Ahmad, Fluid to fluid modeling of critical heat flux, *Int. J. Heat Mass Transfer* **16**, 641–662 (1973).
4. P. Griffith, Correlation of nucleate boiling burnout data, ASME-Paper 57-HT-21 (1957).
5. B. A. Zenkevich, Similitude relations for critical heat loading in forced liquid flow, *Soviet J. At. Energy* **4**, 89–94 (1958).
6. W. R. Gambill, Generalized prediction of burnout heat flux for flowing, subcooled, wetting liquid, *Chem. Engng Prog. Symp. Ser.* **59**(41), 71–87 (1963).
7. Y. Katto, A generalized correlation of critical heat flux for the forced convection boiling in vertical uniformly heated round tubes, *Int. J. Heat Mass Transfer* **21**, 1527–1542 (1978).
8. Y. Katto, An analysis of the effect of inlet subcooling on critical heat flux of forced convection boiling in vertical uniformly heated tubes, *Int. J. Heat Mass Transfer* **22**, 1567–1575 (1979).
9. M. M. Shah, A generalized graphical method for predicting CHF in uniformly heated vertical tubes, *Int. J. Heat Mass Transfer* **22**, 557–568 (1979).
10. Y. Katto, Critical heat flux of forced convection boiling in uniformly heated vertical tubes (Correlation of CHF in HP-regime and determination of CHF-regime map), *Int. J. Heat Mass Transfer* **23**, 1573–1580 (1980).
11. F. Mayinger, Scaling and modeling laws in two-phase flow and boiling heat transfer, in *Two-Phase Flows and Heat Transfer* (edited by S. Kakaç and F. Mayinger), Vol. I, pp. 129–161. Hemisphere, Washington (1977).
12. A. H. Mariy, A. A. El-Shirbini and W. Murgatroyd, Simulation of the region of annular flow boiling in high pressure steam generators by the use of refrigerants, in *Two-Phase Flows and Heat Transfer* (edited by S. Kakaç and T. N. Veziroglu), Vol. III, pp. 1111–1132. Hemisphere, Washington (1977).
13. P. B. Whalley, P. Hutchinson and G. F. Hewitt, The calculation of critical heat flux in forced convection boiling, in *Proc. 5th Int. Heat Transfer Conf.*, Tokyo, Vol. IV, pp. 290–294 (1974).
14. P. B. Whalley, P. Hutchinson and P. W. James, The calculation of critical heat flux in complex situations using an annular flow model, in *Proc. 6th Int. Heat Transfer Conf.*, Toronto, Vol. 5, pp. 65–70 (1978).
15. J. Würtz, An experimental and theoretical investigation of annular steam-water flow in tubes and annuli at 30 to 90 bar, Risø National Lab., Risø Report No. 372 (1978).
16. S. Levy, J. M. Healzer and D. Abdollahian, Prediction of critical heat flux for annular flow in vertical pipes, EPRI NP-1619 (1980).
17. M. El-Shanawany, A. A. El-Shirbini and W. Murgatroyd, A model for predicting the dry-out position by annular flow in a uniformly heated vertical tube, *Int. J. Heat Mass Transfer* **21**, 529–536 (1978).
18. T. Saito, E. D. Hughes and M. W. Carbon, Multi-fluid modeling of annular two-phase flow, *Nucl. Engng Des.* **50**, 225–271 (1978).
19. Y. Katto, General features of CHF of forced convection boiling in uniformly heated vertical tubes with zero inlet subcooling, *Int. J. Heat Mass Transfer* **23**, 493–504 (1980).
20. Y. Katto, On the relation between critical heat flux and outlet flow pattern of forced convection boiling in uniformly heated vertical tubes, *Int. J. Heat Mass Transfer* **24**, 541–544 (1981).
21. A. E. Bergles and M. Suo, Investigation of boiling water flow regimes at high pressure, in *Proc. 1966 Heat Transfer and Fluid Mechanics Institute*, pp. 79–99. Stanford University Press, Stanford (1966).
22. G. F. Hewitt and D. N. Roberts, Studies of two-phase flow pattern by simultaneous X-ray and flash photography, AERE-M 2159 (1967).
23. D. Butterworth and G. F. Hewitt, editors, *Two-Phase Flow and Heat Transfer*. Oxford University Press, Oxford (1977).
24. M. Takada, *Kikai Keisan Ho (Numerical Computation)*, p. 107. Yokendo, Tokyo (1970).
25. G. F. Hewitt and N. S. Hall-Taylor, *Annular Two-Phase Flow*. Pergamon, Oxford (1970).
26. Heat Mass Transfer Section, Scientific Council, Academy of Sciences, U.S.S.R., Tabular data for calculating burnout when boiling water in uniformly heated round tubes, *Thermal Engng* **23**(9), 77–79 (1977).
27. Y. Katto, A study on limiting exit quality of CHF of forced convection boiling in uniformly heated vertical channels, *Trans. Am. Soc. Mech. Engrs.* Series C, *J. Heat Transfer* **104**, 40–47 (1982).

UNE ETUDE ANALYTIQUE DU CHF EN EBULLITION AVEC CONVECTION FORCEE DANS DES TUBES VERTICAUX AVEC UNE REFERENCE SPECIALE AUX GROUPES ADIMENSIONNELS ACTIFS

Résumé—Parmi les quatre régimes caractéristiques qui ont été définis par l'auteur dans une étude précédente sur la formulation générale du flux thermique critique (CHF) deux régimes appelés L et H correspondent à un écoulement annulaire à la sortie du tube. A partir du modèle d'écoulement annulaire développé par Whalley *et al.*, une analyse théorique est faite pour des tubes chauffés emplis d'eau, de R-12 et d'azote liquide saturés ; les résultats obtenus sont comparés avec les formules générales de l'auteur pour clarifier les rôles des groupes adimensionnels. On constate que les groupes adoptés dans le modèle de Ahmad s'accordent avec le modèle annulaire de Whalley *et al.*, qu' un groupe adimensionnel spécial ($\sigma\rho_1/G^2l$) peut être utilisé avec une signification physique en relation avec les données du CHF, et que le transfert massique de gouttelettes entre le film liquide et le noyau gazeux prend des aspects differents entre les régimes L et H.

EINE ANALYTISCHE UNTERSUCHUNG DER KRITISCHEN WÄRMESTROMDICHTE BEIM STRÖMUNGSSIEDEN IN GLEICHFÖRMIG BEHEIZTEN SENKRECHTEN ROHREN UNTER SPEZIELLER BEZUGNAHME AUF DIE MASSGEBLICHEN DIMENSIONSLOSEN GRUPPEN

Zusammenfassung—In einer früreren Veröffentlichung des Autors über die allgemeine Berechnung der kritischen Wärmestromdichte (CHF) wurden vier charakteristische Gebiete klassifiziert. Zweien dieser Gebiete (L- und H-Gebiet benannt) wird am Rohraustritt Ringströmungsform zugeschrieben. Unter Verwendung des Ringströmungs-Modells von Whalley *et al.* wird für gleichförmig beheizte, mit gesättigtem Wasser, R-12 und flüssigem Stickstoff gespeiste Rohre eine theoretische Untersuchung durchgeführt. Die Ergebnisse werden mit der verallgemeinerten Berechnung des Autors verglichen, wobei die Rolle der maßgeblichen dimensionslosen Gruppen herausgearbeitet wird. Es ergibt sich, daß die dimensionslosen Gruppen, die in Ahmads Modell-Gesetz angenommen werden, in Übereinstimmung mit dem Ringströmungs-Modell von Whalley *et al.* sind, daß eine spezielle dimensionslose Gruppe $\sigma\rho_l/G^2l$ mit einer physikalischen Bedeutung bei der Berechnung von CHF-Werten verwendet werden kann und daß der Tröpfchen-Massentransport zwischen dem Flüssigkeitsfilm und der Dampf-Kernströmung verschiedene Erscheinungsformen zwischen dem L- und H-Gebiet annimmt.

АНАЛИТИЧЕСКОЕ ИССЛЕДОВАНИЕ КРИТИЧЕСКОГО ТЕПЛОВОГО ПОТОКА ПРИ КИПЕНИИ ДВИЖУЩЕЙСЯ ЖИДКОСТИ В РАВНОМЕРНО НАГРЕВАЕМЫХ ВЕРТИКАЛЬНЫХ ТРУБАХ. УТОЧНЕНИЕ ОСНОВНЫХ БЕЗРАЗМЕРНЫХ КРИТЕРИЕВ

Аннотация—Установлено, что среди четырех характерных режимов, классификация которых была дана в одной из предыдущих работ автора, в которой было предложено соотношение для расчета критического теплового потока, два режима, а именно L и H, характеризуются кольцевой конфигурацией потока на выходе из трубы. Используя модель кольцевого течения Уолли *и др.*, проведен теоретический анализ для равномерно нагреваемых труб, в которые подается насыщенная вода, фреон-12 и жидкий азот. Проведено сравнение полученных результатов с результатами расчетов по предложенной автором зависимости и выяснена роль основных безразмерных критериев. Установлено следующее: безразмерные критерии, используемые в законе моделирования Ахмада, согласуются с моделью кольцевого течения Уолли *и др.*, безразмерный критерий $\sigma\rho_l/G^2l$ можно физически обоснованно использовать для описания данных по критическому тепловому потоку, между режимами L и H капельный массоперенос между жидкостной пленкой и внутренним объемом газа характеризуется рядом отличительных особенностей.